HARMONIA CA21119

Short-term Scientific Mission Grant

Extended final report

Comparison of AOD and aerosol retrievals collected during the FRC-VI campaign in Davos and validation of improved data processing and calibration algorithms

(22/09/2025 - 10/10/2025)

Grantee: Meritxell Garcia Suñer
Date: 16 October 2025

1. Introduction

Short-Term Scientific Mission (STSM) Grants offer an excellent opportunity for applicants to visit research centers and perform collaborative research focused on a specific topic that aligns with the objective of the COST action. One of the main advantages of these grants is the possibility of face-to-face interaction with supervisors and direct access to the instruments, which fosters communication, facilitates a deeper understanding of the measurement procedures and enhance networking opportunities. The outcomes of each STSM are expected to be included in the deliverables to be submitted periodically by members of the Action.

This particular STSM was focused on the FRC-VI campaign, held in Davos (Switzerland) from 22 September to 10 October and organised by PMOD/WRC. The main objective was to support the applicant's participation in the campaign, allowing her to install and operate the Prede POM-01 sun-photometer from University of Valencia in order to record direct solar irradiance and almucantar radiance data simultaneously with other co-located sun-photometers. This made it possible to obtain a valuable dataset that was later used to compare Aerosol Optical Depth (AOD) and aerosol retrievals between instruments and to validate a new version of the ILP algorithm, recently developed by Gaurav Kumar (from the Solar Radiation Group in Valencia).

During the period covered by the STSM, the grantee gained valuable hands-on experience with the manual operation of the Prede POM-01, including maintenance tasks (e.g. lens cleaning and correct pointing verification), and troubleshooting protocols. The work was supervised by Dr. Stelios Kazadzis and his colleagues at PMOD, especially Natalia Kouremeti and Angelos Karanikolas, who supported the applicant in instrument setup, problem resolution, and daily maintenance. Furthermore, the grantee assisted participants of the IPC XIV campaign and attended the corresponding symposia when the weather conditions did not allow measurements. This provided fundamental knowledge on radiation measurements and instrumentation, including instrument types, configuration, main characteristics, derived products, and the importance of intercomparison and calibration against reference instruments.

Due to the relevance of the results to the MoU T1.1. objective from the WG1 and MoU T2.1 and T2.2 aims from WG2, they will be included in the corresponding deliverable (D2.4), which focuses on uncertainties for optimised and homogenised products and suggestions for improving already existing products. Furthermore, this work will be incorporated into the applicant's PhD thesis, and a scientific publication summarising the main findings is also expected.

2. Results and discussion

In this project, the dataset collected during the FRC-VI campaign has been exploited by comparing the AOD and Ångström Exponent (AE) retrieved from direct irradiance measurements performed with sun-photometers from different aerosol observation networks. In addition, several variants of the ILP algorithm have been tested with the aim of improving its performance in the computation of the calibration coefficients.

The dataset regarded in this analysis covers the period from 22 September to 18 October. However, it should be noted that the FRC-VI campaign was extended, so the instruments kept collecting data at the end of the STSM period. The whole data set will be analysed once the Prede sky-radiometers are dismounted and returned to their respective sites. In the case of the POM-01 from the University of Valencia, we expect to include posterior Improved Langley Plot calibrations performed at Valencia, so we can take into account seasonality and site dependencies.

This report is structured in four parts. First, a brief description of the campaign and the main issues encountered is provided. Then, the analysis will focus on the intercomparison of AOD and AE retrieved from sun-photometers belonging to different networks (Cimel, AERONET; Prede, SKYNET; PFR, GAW). The third part explores possible improvements to the standard ILP method and evaluates the new version proposed by Gaurav Kumar, thus assessing the impact of calibration coefficients on the computation of AOD. Finally, the main findings are summarised in the conclusions, as well as the perspectives for future work.

2.1 The FRC-VI campaign

The FRC-VI (Filter Radiometer Comparison) campaign took place in Davos, Switzerland, and was hosted at PMOD/WRC from 22 September to 10 October, 2025. It was held in parallel with the IPC-XIV (International Pyrheliometer Comparison) and the IPgC-IV (International Pyrgeometer Comparison). These intercomparisons are organised every 5 years, bringing together national meteorological centres and manufacturers of radiometric equipment to calibrate their instruments against the reference. Afterward, these centres are responsible for organising calibration campaigns to ensure traceability within their respective regions.

Regarding the FRC-VI, several sun-photometers from different aerosol observation networks participated in the campaign: 11 PFR, 4 Cimel, 2 CW193 and 3 Prede POM, among others (Figure 1a). In particular, for the Prede instruments, one was the lunar POM-01 from Tor Vergata (hereafter referred to as the CNR Prede to distinguish it from the Valencia POM-01, referred to as the UVEG Prede), and the third was a POM-02 belonging to the Japan Meteorological Agency. These are shown in Figures 1b and 1c.

Unfortunately, weather conditions were generally unfavourable, with many days affected by rain, snow or cloud cover. Nevertheless, two exceptionally clear days with pristine atmosphere after aerosols being washed away by rain, 28 and 29 September, were crucial for collecting high-quality measurements. Additional days with relatively clear skies were 2 and 3 October. These conditions allowed the performance of tests such as X-scans to verify the correct pointing of the UVEG Prede. In addition, solar disk scans performed on 28 September enabled the computation of a new value of the Solid View Angle (SVA), which is expected to improve the performance of the ILP, as it will be discussed in Section 2.3. Some hours of data were also collected on partially cloudy days that offered occasional clear skies windows, such as 23 and 26 September and 8 October.

Due to the limited number of days with completely clear skies, and given that very good weather conditions were forecast after the official campaign period, it was decided to extend the measurements. Therefore, most of the instruments, including the three Prede, continued to record data at the time this report was prepared.

Several issues affected both the CNR and the UVEG Prede instruments. The most severe incident occurred when attempting to connect both the UVEG and CNR Prede to the same laptop after the official end of the FRC period. During a control test, the UVEG collimator, which was performing its setup routine, collided with the CNR collimator, moving the UVEG Prede base. This incident significantly affected the UVEG Prede movement, so it had to be aligned and leveled again. In addition, pointing issues with the UVEG Prede were subsequently detected, thus requiring continuous surveillance to manually correct the deviation (e.g. a 2º offset was applied on 15 October), resulting in the loss of two days of measurements (9 and 10 October). Although a thorough examination of the instrument will be carried out once the instrument returns to Valencia, we believe the malfunction to be related to the transmission belt (which had caused some problems in the past) preventing proper motion. Other minor issues that could be quickly solved were sky-radiometer control software freezing requiring a restart (12 October), unexpected laptop shutdown, and the correction of the instrument's north alignment during the first two days of the campaign.

The CNR Prede also experienced a communication error on 12 October, which was attributed to a cable connection failure. The problem was resolved by reconnecting the cables, although measurements during that morning could not be recorded.

Despite these difficulties, and although a significant amount of data could not be recorded, the experience proved to be a good practice for the applicant in learning how to cope with these issues. Then, she gained skills on the identification of the problem source as well as some resolution methods. In addition, the applicant learnt about daily maintenance of the instrument such as daily checks and cleaning every morning from September 25 onward.

Figure 1: Pictures taken during the FRC-VI campaign: (a) Some of the instruments that participated in FRC-VI, on a snowy day (6 October). (b) The UVEG Prede. The CW193 can be seen behind it, in the upper part of the picture. (c) The three Prede that participated in the campaign, together with several PFR.

2.2 AOD and Ångström Exponent comparison

In this section, the intercomparison of the AOD and AE obtained from the UVEG and CNR Prede measurements with the values retrieved from the instruments in the other networks (Cimel – AERONET; PFR - GAW) is performed. In addition, the UVEG and CNR Prede are also compared with each other, and analogously for the Cimel and the PFR.

The agreement between the retrievals is based on the comparison of four statistical parameters. For each pair of instruments, the set of data points that is used in the comparison is built based on a simultaneity criterion. In particular, only those two data points from each instrument whose time difference is less than or equal to 30 s, i.e. $\Delta t \leq 30\, s$, are considered in the computation of the statistics.

Given a set of values x constituted by N measurements of a certain parameter, $x \equiv \{x_1, x_2, \ldots, x_N\}$ that are considered pairwise simultaneous to the set of retrievals y of the same magnitude from another instrument, $y \equiv \{y_1, y_2, \ldots, y_N\}$; the Root-Mean-Square Error (RMSE) is defined as

$$RMSE\,(x,y) = \sqrt{\frac{\sum_{i=1}^{N}(x_i - y_i)^2}{N}}\ . \qquad (1)$$

The standard deviation of the differences, $\delta_i \equiv |x_i - y_i|$ are

$$std\,(\delta) = \sqrt{\frac{\sum_{i=1}^{N}\left(\delta_i - \bar{\delta}\right)^2}{N}}\ , \qquad (2)$$

being $\bar{\delta}$ the mean of these differences. The two statistical parameters above allow us to measure the discrepancies between the compared values. Specifically, the RMSE accounts for the total error between measurements, while $std(\delta)$ quantifies the variability of the differences. The Mean Bias Deviation (MBD),

$$MBD\,(x,y) = \frac{\sum_{i=0}^{N-1}(x_i - y_i)}{N}\ , \qquad (3)$$

measures the average difference between the two sets of values. Finally, the correlation coefficient R^2, computed as

$$R^2\,(x,y) = \left(\frac{\sum_{i=1}^{N}(x_i - \bar{x})(y_i - \bar{y})}{\sqrt{\sum_{i=1}^{N}(x_i - \bar{x})^2 \sum_{i=1}^{N}(y_i - \bar{y})^2}}\right)^2\ , \qquad (4)$$

measures the strength of the linear relationship between the sets of measurements *x* and *y*. The statistical parameters defined above quantify the discrepancies between the different instruments, thus complementing the qualitative study of the intercomparison between instruments based on scatter plots.

Table 1: Nominal wavelengths available for each instrument compared in this study. The green cells indicate the channels that have been used for the intercomparison between instruments.

	Wavelength (nm)										
Prede	340			400			500	675	870	1020	
Cimel	340		380			440	500	675	870	1020	1640
PFR		370			410		500		870		

Nevertheless, these intercomparisons are limited to the coincident wavelengths available for each pair of instruments, as outlined in Table 1. Hence, the comparison between Prede and Cimel can be carried out at 340, 500, 675, 870 and 1020 nm, while comparisons between Prede and Cimel with PFR are limited to wavelengths of 500 and 870 nm.

In the case of the comparisons involving the Cimel sun-photometer[1], the differences between simultaneous measurements have also been analysed. Furthermore, their agreement has been evaluated using the WMO limits, which depend on the optical air mass *m* and are defined as:

$$WMO_{\pm}(m) = \pm\,(0.005 + \frac{0.001}{m})\ , \qquad (5)$$

where + and – represent the upper and lower limits, respectively. These limits are used to assess kind of traceability of an instrument: if AOD differences fall within the interval defined by these limits, the instrument is considered traceable.

It is important to note that, for the UVEG Prede, several computations of the calibration coefficients have been carried out. However, in this section only the AOD and AE derived using Gaurav Kumar's version of the ILP algorithm are presented. In addition, the 340 nm channel is excluded. The reason for this is that this filter appears to be degraded, and its poor performance affects the computation of the calibration coefficients in the other channels. In contrast, the standard ILP calibration method has been applied to the CNR Prede. The impact of the calibration method on AOD and AE retrievals will be discussed in Section 2.3.

---

[1] *The analysis involving WMO limits for comparisons with respect to the PFR will also be carried out in the near future.*

2.2.1. UVEG-CNR Prede comparison

Table 2a shows the values of the statistical parameters defined in Eq. 1-4 above obtained for the simultaneous AOD and AE data points from the Prede. To perform this comparison, negative and NaN data points of AOD and AE are removed. Focusing on the small values of the RMSE and standard deviation of the differences at 400, 500, 675 and 870 nm, it can be stated that the measurements are compatible. However, the RMSE for AOD_{1020} is very large, indicating that there may be a problem with this channel. The AE is calculated based on AOD, so the error propagates, thus explaining why larger values are obtained for the statistic parameters. Initially, the AE for Prede was computed using the AOD at 1020 nm, but after concluding that there was an issue with this channel, the AE was recalculated using other channels.

With regard to the MBD, it should be noted that the values at 400, 500, 675, 870 and 1020 nm are negative, indicating that the CNR Prede tends to retrieve higher AOD than UVEG (see Figure 2a). In fact, Figure 2b, which shows the evolution of AOD throughout 17 October, clearly illustrates this behaviour. On the other hand, the MBD is higher at 1020 nm, which is not an unexpected result considering what has been observed for the other statistical parameters. As for the AE parameter, the MBD values are positive and higher than those of AOD, indicating higher AE derived from the UVEG Prede and, therefore, greater differences in AOD at 400-500nm, 400-675nm and 400-870nm.

Finally, the R^2 values indicate a considerable discrepancy between UVEG and CNR Prede retrievals, with the highest correlations for AOD_{400}, AOD_{500}, $AE_{400-500}$ and $AE_{400-675}$. Even though AOD_{1020} shows a high R^2 compared to the other variables, this channel differs significantly from the other instruments in the case of the two Prede, and therefore requires further attention, as will be discussed in the following subsections.

Figures 3a and 3b show the evolution of AOD at all available wavelengths throughout the campaign for the UVEG and CNR Prede, respectively. The gaps correspond to rainy and cloudy days when measurements could not be performed. Overall, the AOD is quite low, which corresponds to a mountain site such as Davos after a rainy episode. The unexpected behaviour of the 1020 nm channel is clearly distinguished in both cases, as the AOD normally decreases with increasing wavelength, but a considerable increase is observed instead. This behaviour is even more pronounced in the case of the CNR Prede, as seen in Figure 3b.

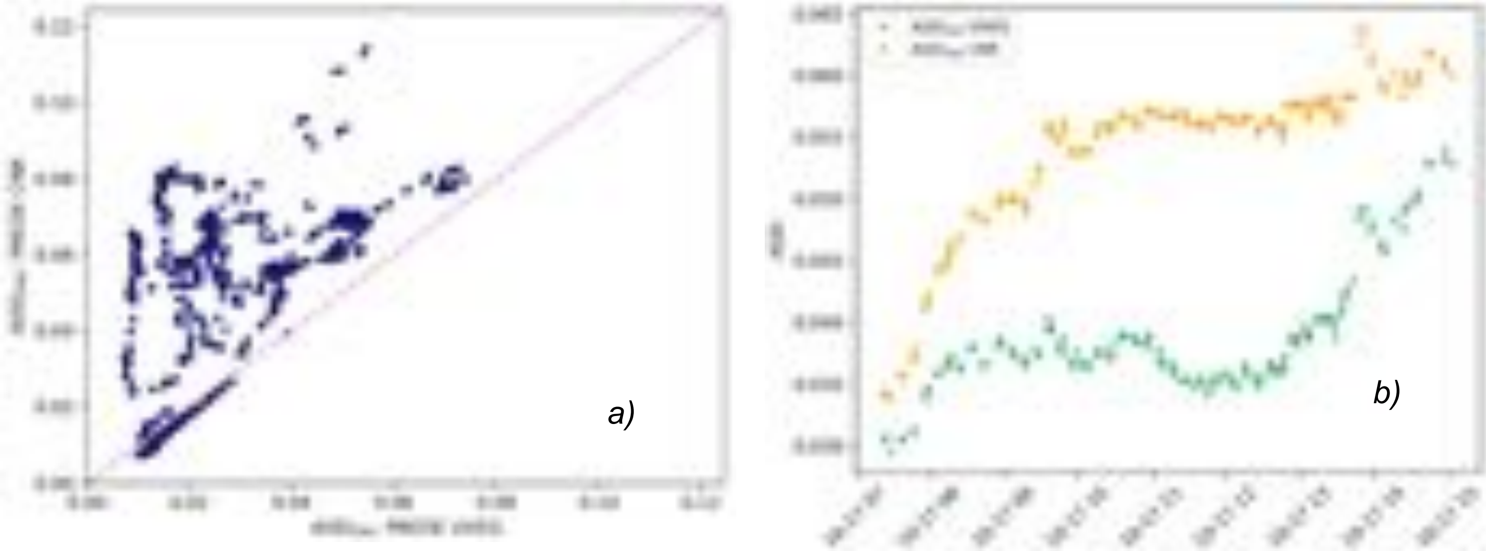

Figure 2: Results from the comparison of the AOD_{500} retrieved by the UVEG and the CNR Prede. In particular, the scatter plot obtained (a) and the evolution of AOD on 17 October (b) are shown.

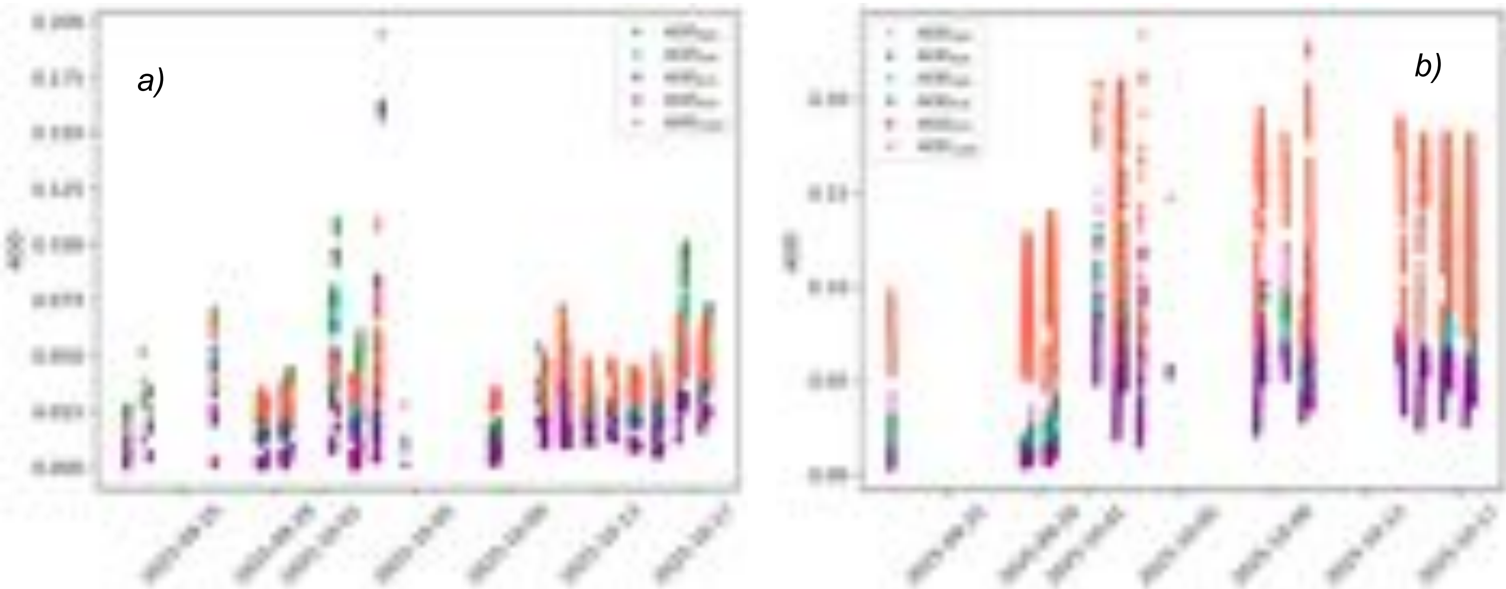

Figure 3: Evolution of the AOD values retrieved from the UVEG (a) and CNR (b) Prede throughout the campaign (22 September to 18 October), for every available wavelength.

2.2.2. UVEG Prede-PFR comparison

The AOD and AE derived from raw data collected by the UVEG Prede have been compared with those from the SE-SMHI PFR. The results are shown in Table 2b and Figure 4. As mentioned above, the comparison could only be performed at the 500 and 870 nm wavelengths. According to the RMSE and the standard deviation of the differences, the discrepancies between the AOD are relatively small. These are slightly larger in the case of the AE, although this is an expected result from a derived magnitude that has not been calculated using the same wavelength range.

The negative MBD values imply slightly higher AOD values in the case of the UVEG Prede. The opposite is observed for the $AE_{400-675}$, thus indicating a lower $AE_{400-675}$ calculated from the UVEG Prede.

As for the R^2 values, these are relatively low, indicating a weak correlation between the retrieved AOD and AE. In fact, Figure 4a shows several outliers that significantly affect the comparison. Since these anomalous points correspond to different days, they require a more detailed examination. This suggests that the PFR dataset still needs further cleaning, which would likely lead to a great improvement in the intercomparison results. Finally, it is worth noting that the temporal evolution of the PFR AOD throughout the campaign (Figure 4b) exhibits a clear pattern, with AOD decreasing as wavelength increases.

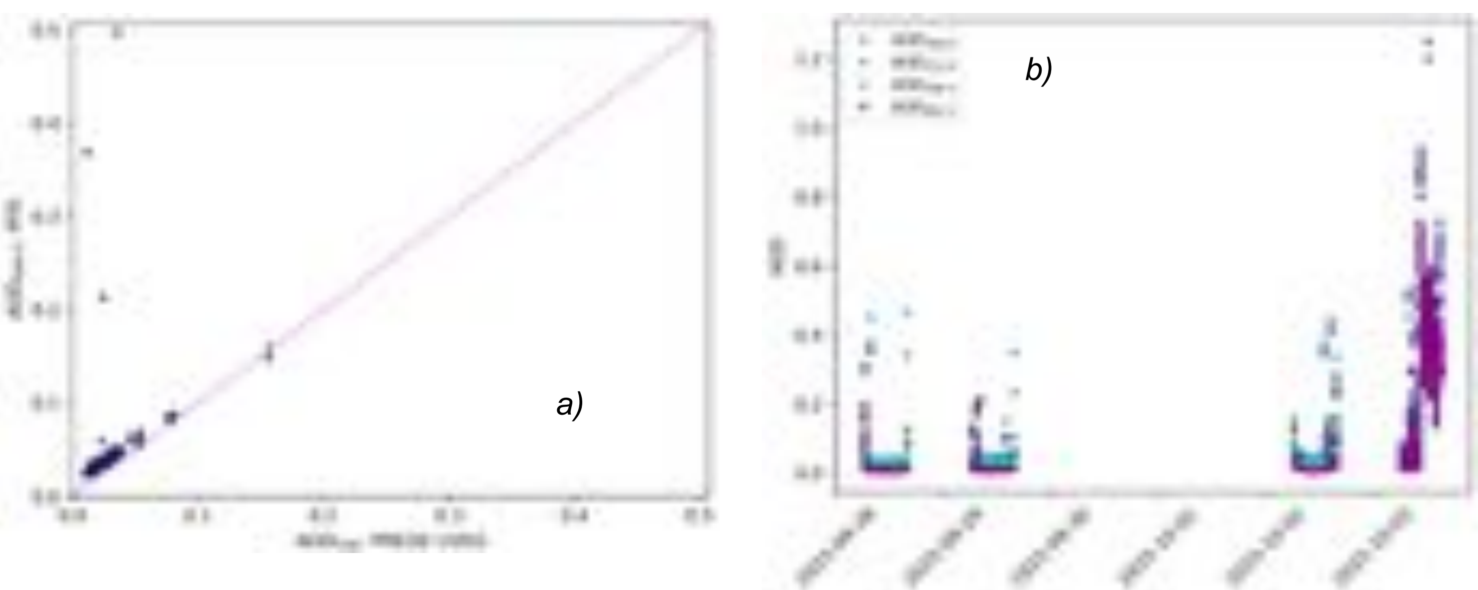

Figure 4: (a) Scatter plot from the comparison of the AOD_{500} retrieved by the UVEG Prede and the PFR. (b) Evolution of the AOD values retrieved from the PFR for the days of available data (28 and 29 September, as well as 2 and 3 October), and for every wavelength.

2.2.3. UVEG Prede-Davos Cimel comparison

To complete the intercomparison study related to the UVEG Prede, level 1.5 AOD and AE products from AERONET for the Cimel in Davos have been compared with the Prede values. The results are shown in Table 2c. The RMSE and standard deviation of the differences are consistent with the combined error associated with AOD measurements for the Cimel, ± 0.01 (Holben et al., 1998; Sinyuk et al., 2020) and Prede ± 0.02 (Campanelli et al., 2004). Furthermore, as noted above, the discrepancies related to the AOD_{1020} channel are greater, as it is the case for the AE. However, it should be noted that AERONET provides $AE_{440-870}$, while the Prede measures at 400 nm, so the $AE_{400-870}$ is alternatively obtained instead.

The MDB values in Table 2c are small, which supports the idea of compatibility between the retrievals of both instruments. This agreement can be also observed in Figure 5a. The larger discrepancy in MDB (except for the case of the AE, already discussed), corresponds to the 1020 nm channel. When comparing the evolution of the AOD of both instruments, i.e., Figures 3a and 5b for Prede and Cimel, respectively, the problem of Prede's overestimation of AOD_{1020} is clearly identified. This can be attributed to filter degradation or to the computation of the calibration coefficient. However, the first hypothesis seems more feasible, since if the problem were due to calibration, greater discrepancies would be expected for the other channels. More investigation is then needed for this channel.

The R^2 values are relatively small, with the highest being that of the correlation with AOD_{500}. Despite this, the agreement is better than with the PFR and the CNR Prede.

Finally, the traceability of the UVEG Prede has been analysed based on WMO limits defined in Eq. 5. The proportion of AOD differences falling within the range of values delimited by the WMO limits is shown in Table 2c. As expected based on the previous study, satisfactory results are obtained for the 500, 675 and 870 nm channels, with 96%, 77% and 88% of data points within the range (see Figure 5c). However, AOD_{1020} differences are too large, with only 3% of the points showing agreement between the instruments. The non-traceability of the 1020 nm channel confirms the need for investigate the temporal evolution of the calibration coefficients for this channel and attempt to assess the origin of the problem with this filter.

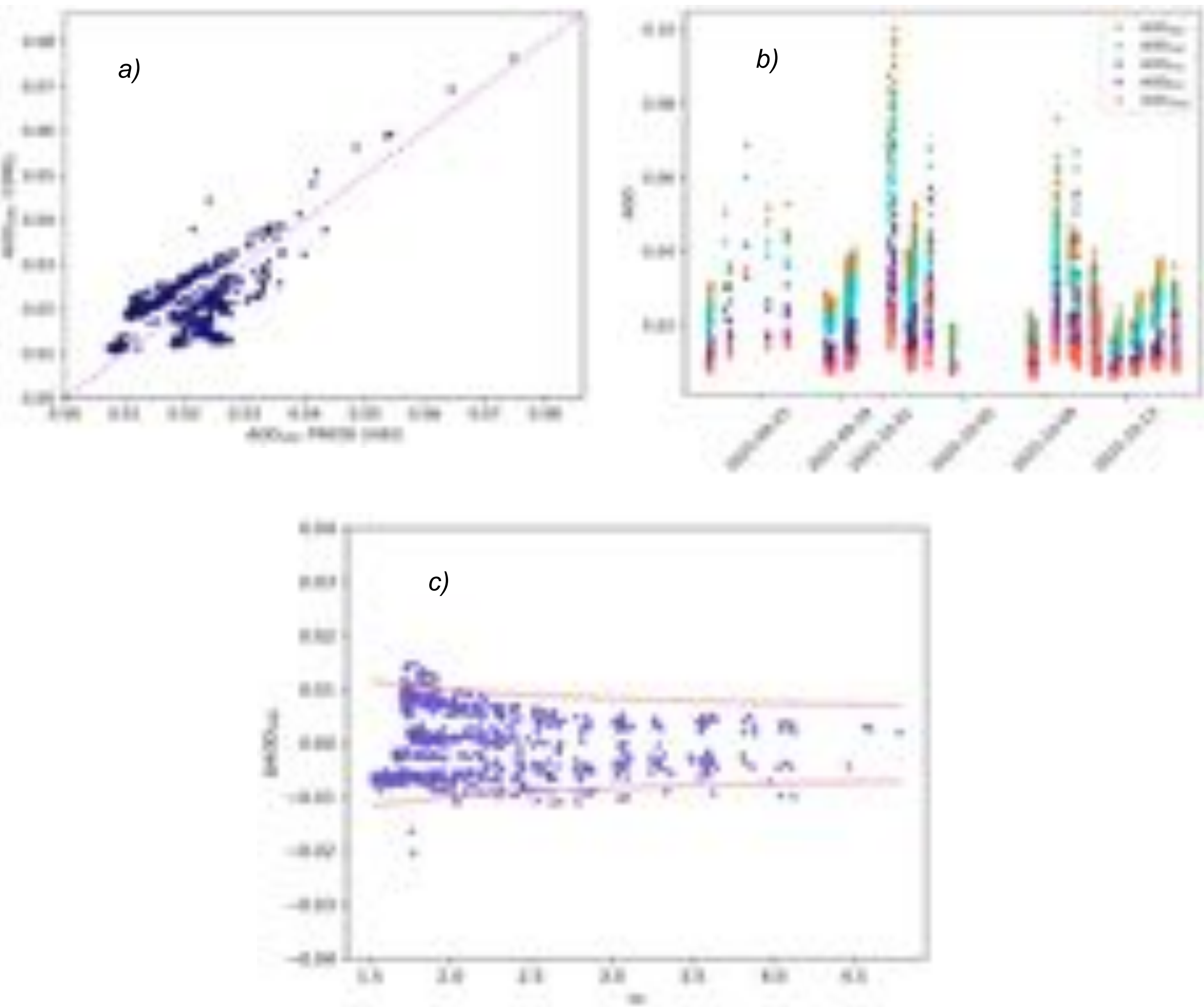

Figure 5: (a) Scatter plot from the comparison of the AOD_{500} retrieved by the UVEG Prede and the Cimel. (b) Evolution of the AOD values retrieved from the Cimel for the days of available data (from 22 September to 15 October), and for every wavelength. (c) AOD_{500} differences for Cimel and UVEG Prede as a function of the optical air mass. Upper and lower WMO limits are also indicated.

2.2.4. Davos Cimel-CNR Prede comparison

This section focuses on the comparison between the retrievals from the CNR Prede and the Cimel in Davos. Based on Table 3a, the agreement between AOD retrievals from both instruments lies at the limit of the Cimel's estimated uncertainty. The RMSE and the standard deviation of the differences increase slightly at longer wavelengths. As also observed for the UVEG Prede, the 1020 nm channel is characterised by a large RMSE and by the unexpected behaviour of AOD_{1020} in Figure 3b. This could indicate severe filter degradation, suggesting the need for a more exhaustive analysis. However, coincidence with the UVEG Prede deter us not to rule out a problem in the calibration application, to be double checked in the future. As expected, the RMSE and $std(\delta)$ for the AE are larger than for the AOD.

According to the MBD in Table 3a and Figure 6a, the CNR Prede tends to retrieve higher AOD values and lower AE. The R^2 values indicate a poor correlation, with the highest value corresponding to AOD_{340}. It therefore appears that the AOD and AE retrieved from the UVEG Prede measurements show a better agreement with the Cimel than those obtained from the CNR Prede. It should be noted, however, that for the UVEG Prede the calibration coefficients were computed based on a new version of the ILP algorithm, whereas for the CNR Prede, they were obtained using the standard ILP procedure. The effect of the calibration method on the UVEG Prede results is studied in Section 2.3.

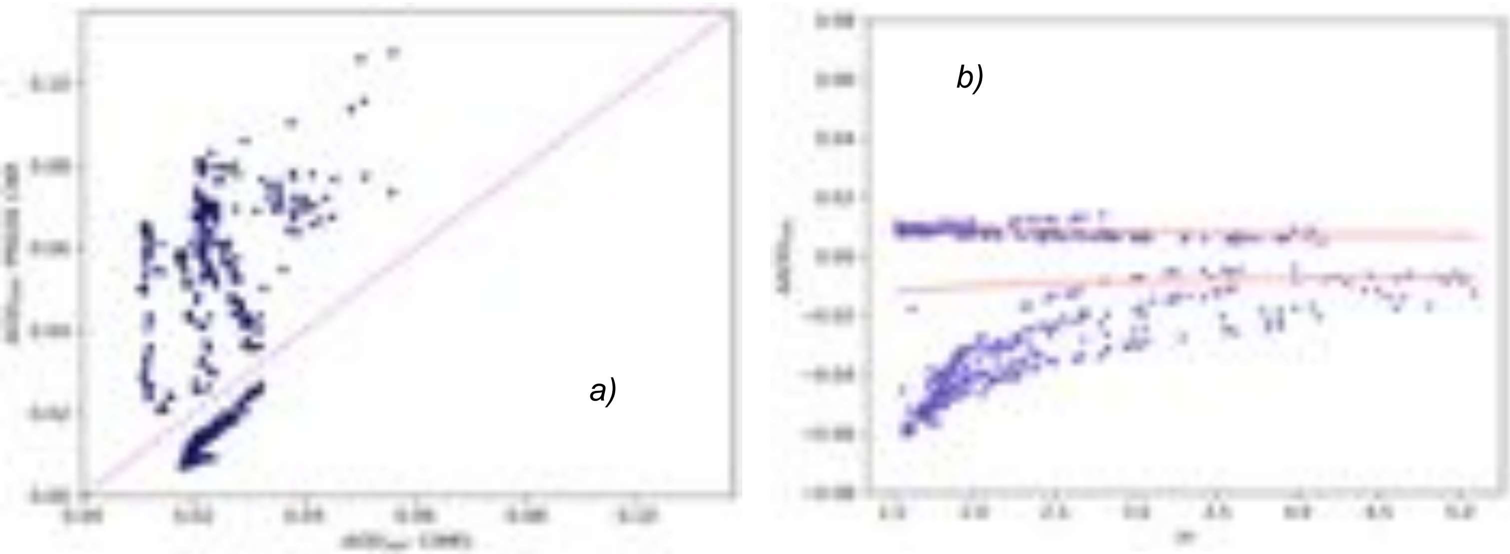

Figure 6: (a) Scatter plot from the comparison of the AOD_{500} retrieved by the CNR Prede and the Cimel. (b) AOD_{500} differences for Cimel and CNR Prede as a function of the optical air mass. Upper and lower WMO limits are also indicated.

Table 3: Summary of the statistical parameters defined in Eq. 1-5 applied to the comparison of the AOD and AE from the CNR Prede with the values from the other instruments, at the available wavelengths (see Table 1): (a) Davos Cimel –CNR Prede; (b) PFR – CNR Prede.

	Davos Cimel–CNR Prede				
a)	$RMSE$	$std(\delta)$	MBD	R^2	WMO (%)
AOD_{340}	0.03	0.02	-0.02	0.33	26
AOD_{500}	0.03	0.02	-0.02	0.07	35
AOD_{675}	0.04	0.02	-0.03	0.02	36
AOD_{870}	0.04	0.03	-0.03	0.03	36
AOD_{1020}	0.13	0.04	-0.12	0.01	0
$AE_{400-675}$	0.94	0.43	0.82	0.01	0
	PFR –CNR Prede				
b)	$RMSE$	$std(\delta)$	MBD	R^2	
AOD_{500}	0.03	0.02	0.00	0.06	
AOD_{870}	0.03	0.03	-0.01	0.00	
$AE_{400-675}$	1.21	0.44	1.13	0.03	

Regarding the traceability of the CNR Prede, (Table 3a and Figure 6b), no channel shows at least 50% of the AOD differences within the WMO limits. The highest percentages are 36% at 675 nm and 870 nm, and 35% for AOD_{500}. The 1020 nm channel deserves particular attention, as not a single point lies within the WMO limits, confirming the non-traceability of this quantity.

2.2.5. PFR–CNR Prede comparison

The CNR Prede retrievals have also been compared with the PFR products (see Table 3b). The RMSE values and standard deviation of the differences for the AOD are similar to those in the previous comparison with Cimel. In addition, AE also shows higher values for RMSE, $std(\delta)$ and MBD compared to AOD. The low MBD values for AOD in Table 3b can be understood by looking at Figure 7. However, the correlation between these quantities is very poor.

Therefore, based on the comparisons of CNR Prede with instruments from other networks, it can be stated that improvements in the retrievals are necessary. This could be achieved by recalculating the calibration coefficients using Gaurav Kumar’s version of

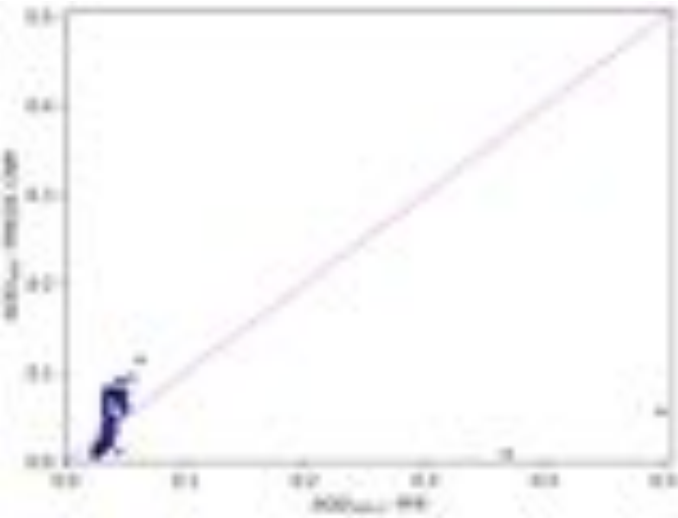

Figure 7: Scatter plot from the comparison of the AOD_{500} retrieved by the CNR Prede and the PFR.

the ILP algorithm, as was done for UVEG Prede, as well as a characterising the filter response to confirm the degradation hypothesis, so there is still room for improvement.

2.2.6. Davos Cimel-PFR comparison

Finally, as a matter of exercise, an intercomparison between AERONET AOD and AE products from the Cimel with the AOD and AE retrievals from the PFR has been carried out. The corresponding statistical values are presented in Table 4. As in the case of the Prede, the only channels available for comparison are 500 and 870 nm. A good agree-

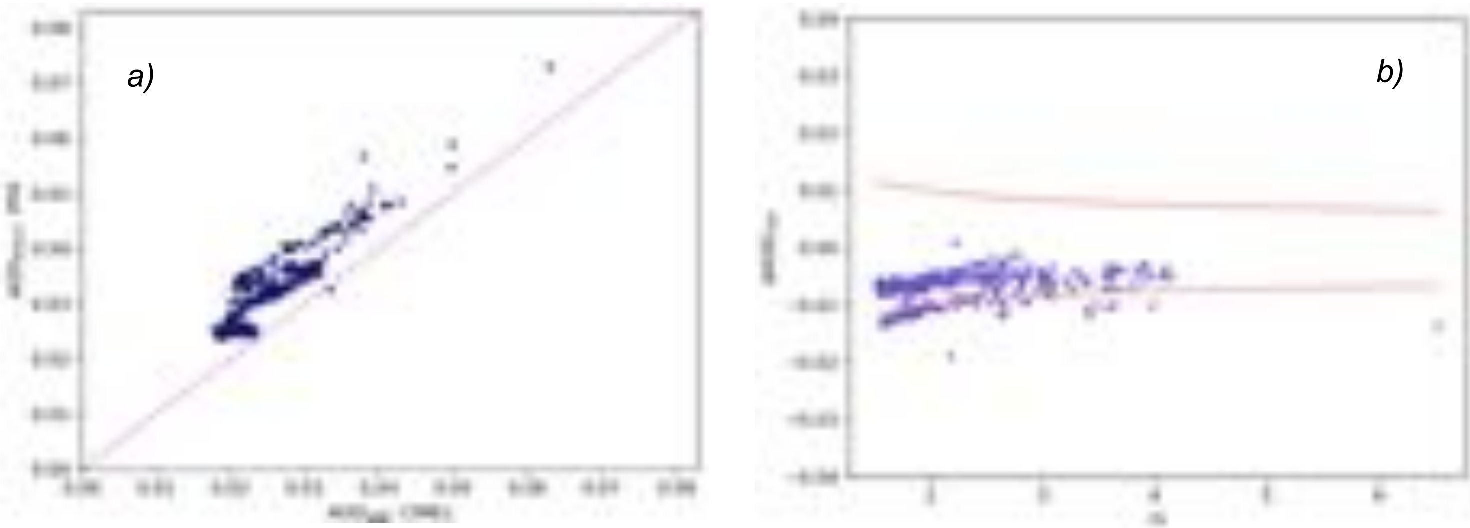

Figure 8: (a) Scatter plot from the comparison of the AOD_{500} retrieved by the PFR and the Cimel. (b) AOD_{500} differences for Cimel and PFR as a function of the optical air mass. Upper and lower WMO limits are also indicated.

Table 4: Summary of the statistical parameters defined in Eq. 1-5 applied to the comparison of the AOD and AE from the Cimel at the Davos AERONET station and the SE-SMHI PFR, for the available wavelengths (see Table 1).

	Davos Cimel - PFR				
	$RMSE$	$std(\delta)$	MBD	R^2	WMO (%)
AOD_{500}	0.01	0.00	-0.00	0.81	76
AOD_{870}	0.00	0.00	0.00	0.90	100
$AE_{440-870}$	0.47	0.17	-0.44	0.38	-

ment is observed for the AOD retrievals from both instruments, particularly at 870 nm, whereas larger discrepancies are found for the AE, as expected. This agreement is illustrated in the scatter plot in Figure 8a. Regarding traceability, most of the AOD differences fall within the WMO limits for both the 500 and 870nm channels (Figure 8b). Overall, the agreement between the Cimel and PFR retrievals is confirmed, supporting the use of these instruments for comparing AOD and AE values derived from Prede measurements. These results are to be considered preliminary, given that the data still did not reach level 2.

2.3 Effects of the calibration procedure in the retrievals

In this section, we examine the influence of the calibration method on the computation of AOD and the AE from the raw Prede data. In particular, we analyse measurements from the UVEG Prede by implementing four versions of the ILP calibration method (Nakajima et al., 2020), each introducing a particular modification. Each version is based on a specific hypothesis aimed at improving the Cimel-Prede intercomparison results. The performance of each modified procedure is then evaluated and compared with the results obtained from the other calibration approaches.

2.3.1 Original calibration: Improved Langley Plot

The first calibration applied was the official version of the Improved Langley Plot. The calculated AOD and AE values are compared with the AERONET measurements from the Cimel, as well as with the values provided from the raw measurements of the PFR and the CNR Prede. The corresponding statistical parameters are summarised in Table 5. Significant discrepancies are observed in both AOD and AE, particularly for the

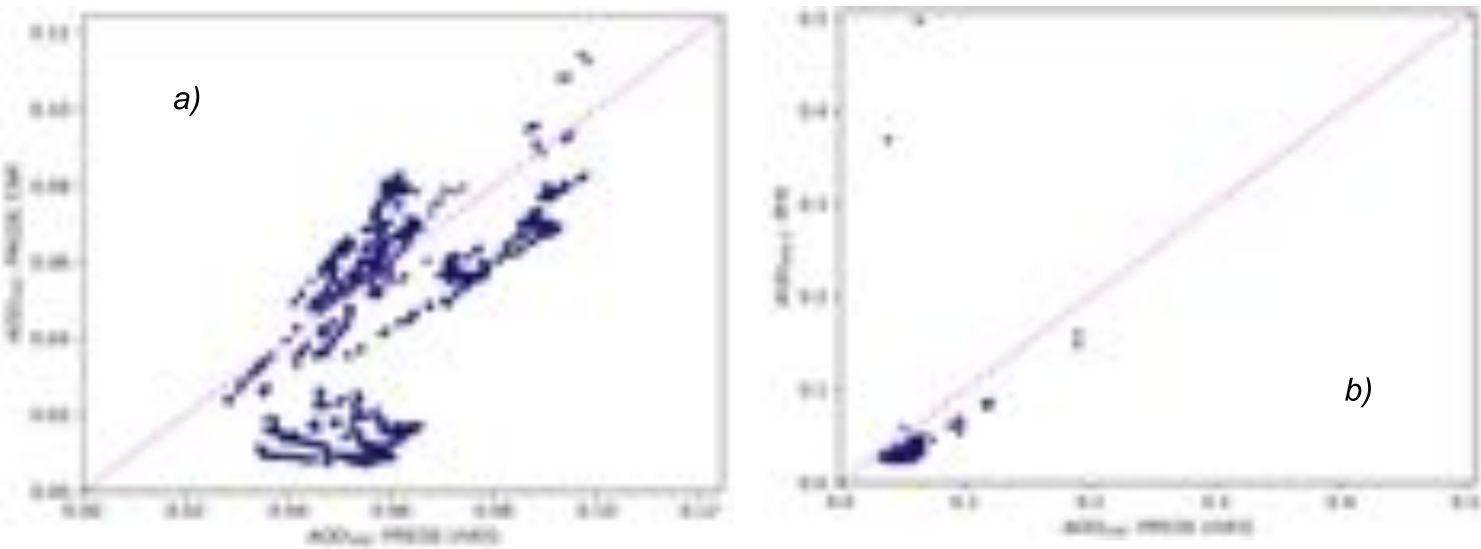

Figure 9: Scatter plot from the comparison of the AOD_{500} retrieved by the UVEG Prede and the (a) CNR Prede; (b) PFR.

UVEG-CNR Prede and the UVEG Prede–Cimel Davos comparisons. In fact, considering the low correlation coefficients R^2 in Table 5, the AOD and AE values cannot be regarded as compatible. This is clearly illustrated in Figures 9a, 9b and 10a at 500 nm. The same conclusion applies to the traceability (Figure 10b): only the AOD values at 870 nm from the UVEG Prede fall within the WMO limits when compared to the Cimel (see Table 5c).

The 1020 nm and especially the 340 nm channels require closer examination, as they tend to highly overestimate the AOD. Moreover, the malfunction of these channel, that may be caused by filter degradation, may also affect the retrievals at other wavelengths. Therefore, the next step is to apply the ILP method excluding the 340 nm channel and evaluate whether the results improve.

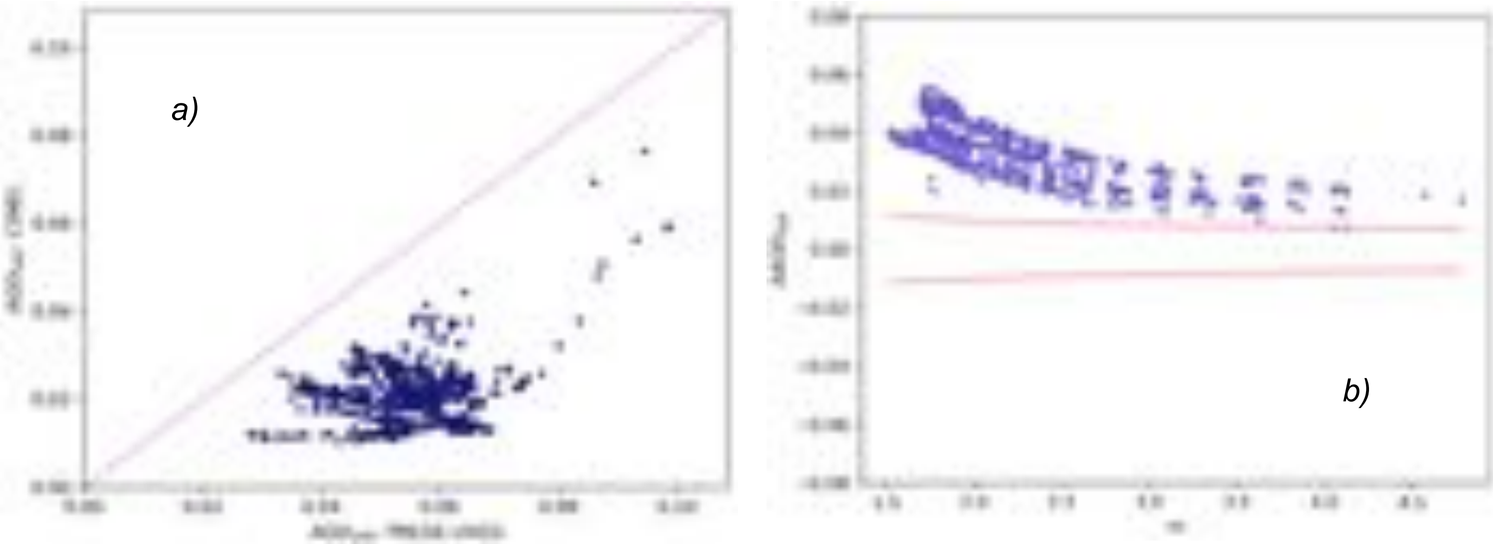

Figure 10: (a) Scatter plot from the comparison of the AOD_{500} retrieved by the UVEG Prede and the Davos Cimel. (b) AOD_{500} differences for the Cimel and the UVEG Prede as a function of the optical air mass. Upper and lower WMO limits are also indicated.

Table 5: Summary of the statistical parameters defined in Eq. 1-5 applied to the comparison of the AOD and AE from the UVEG Prede with the values from the other instruments, at the available wavelengths (see Table 1): (a) UVEG Prede-CNR Prede; (b) UVEG Prede-PFR; and (c) UVEG Prede-Cimel. The standard ILP has been used in the computation of the UVEG Prede's calibration coefficients.

UVEG Prede-CNR Prede					***UVEG Prede –SE SMHI PFR***				
a)	$RMSE$	$std(\delta)$	MBD	R^2	b)	$RMSE$	$std(\delta)$	MBD	R^2
AOD_{340}	0.25	0.06	0.25	0.02					
AOD_{400}	0.06	0.02	0.06	0.26					
AOD_{500}	0.02	0.01	0.01	0.30	AOD_{500}	0.03	0.02	0.02	0.09
AOD_{675}	0.02	0.01	-0.01	0.18					
AOD_{870}	0.04	0.02	-0.03	0.16	AOD_{870}	0.02	0.02	-0.00	0.17
AOD_{1020}	0.11	0.03	-0.10	0.30					
$AE_{400-500}$	2.06	0.57	1.98	0.09					
$AE_{400-675}$	1.72	0.42	1.67	0.05	$AE_{400-675}$	1.22	0.29	1.18	0.57
$AE_{400-870}$	2.18	0.68	2.07	0.06					

UVEG Prede–Davos Cimel					
c)	$RMSE$	$std(\delta)$	MBD	R^2	WMO (%)
AOD_{340}	0.27	0.06	0.27	0.01	0
AOD_{500}	0.04	0.01	0.03	0.09	0
AOD_{675}	0.02	0.01	0.02	0.11	4
AOD_{870}	0.01	0.00	0.00	0.18	83
AOD_{1020}	0.03	0.01	0.03	0.17	4
$AE_{400-675}$	1.36	0.45	1.28	0.25	-

2.3.2 Improved Langley Plot without 340 nm

As suggested in the previous subsection, the AOD and AE have been recalculated and the intercomparison analysis is repeated, this time excluding the 340 nm channel. The resulting statistical parameters are summarised in Table 6. When compared with Table 5, the improved agreement between the AOD and AE derived from the UVEG Prede and those obtained from the PFR and Cimel is clearly noticeable. In particular, the RMSE, $std(\delta)$ and MBD values are slightly reduced with this new calibration, and the correlation coefficients also indicate better consistency between the retrievals. This improvement is illustrated in Figures 11a, 11b and 12a. Moreover, Figure 12b shows enhanced traceability for all channels except 870 nm (Table 6c), for which the percentage of points within the WMO limits is slightly reduced. However, the 1020 nm channel continues to exhibit large discrepancies between the Prede and the Cimel.

Assuming that these behaviours are associated with filter degradation, the next step will be to compute new values of the Solid View Angle (SVA), which are expected to compensate for the changes in the filter response over time.

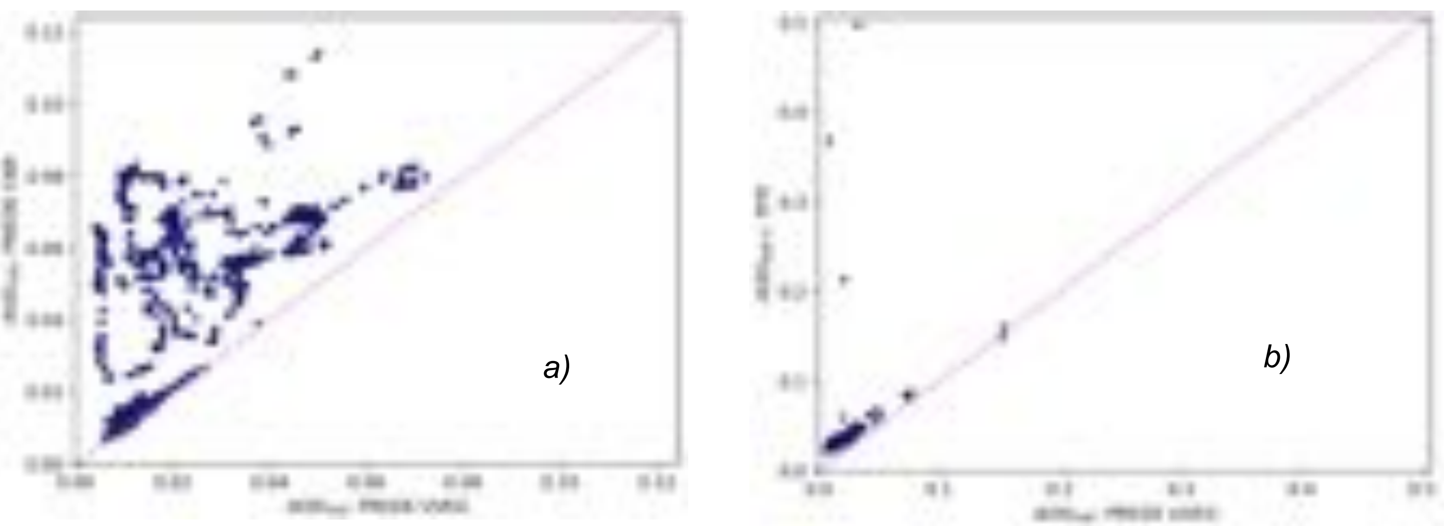

Figure 11: Scatter plot from the comparison of the AOD_{500} retrieved by the UVEG Prede and the (a) CNR Prede; (b) PFR.

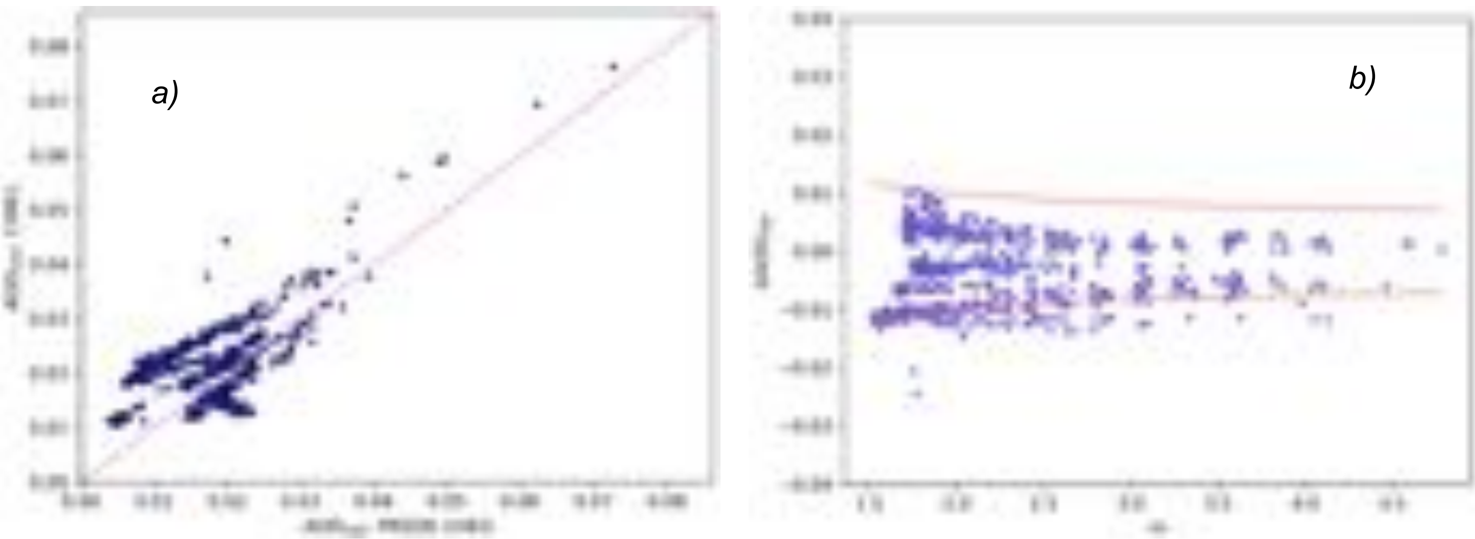

Figure 12: (a) Scatter plot from the comparison of the AOD_{500} retrieved by the UVEG Prede and the Davos Cimel. (b) AOD_{500} differences for the Cimel and the UVEG Prede as a function of the optical air mass. Upper and lower WMO limits are also indicated.

Table 6: Summary of the statistical parameters defined in Eq. 1-5 applied to the comparison of the AOD and AE from the UVEG Prede with the values from the other instruments, at the available wavelengths (see Table 1): (a) UVEG Prede-CNR Prede; (b) UVEG Prede-PFR; and (c) UVEG Prede-Cimel. The standard ILP has been used in the computation of the UVEG Prede's calibration coefficients, but the 340 nm channel has not been regarded in the calculation.

UVEG Prede-CNR Prede					**UVEG Prede –SE SMHI PFR**				
a)	$RMSE$	$std(\delta)$	MBD	R^2	b)	$RMSE$	$std(\delta)$	MBD	R^2
AOD_{400}	0.03	0.02	-0.02	0.32					
AOD_{500}	0.03	0.02	-0.03	0.24	AOD_{500}	0.03	0.02	-0.02	0.18
AOD_{675}	0.03	0.02	-0.03	0.14					
AOD_{870}	0.04	0.02	-0.04	0.16	AOD_{870}	0.03	0.03	-0.01	0.15
AOD_{1020}	0.11	0.03	-0.10	0.28					
$AE_{400-500}$	1.48	0.71	1.30	0.23					
$AE_{400-675}$	0.70	0.34	0.61	0.25	$AE_{400-675}$	1.45	0.98	1.05	0.29
$AE_{400-870}$	1.73	0.97	1.43	0.28					

UVEG Prede–Davos Cimel					
c)	$RMSE$	$std(\delta)$	MBD	R^2	WMO (%)
AOD_{500}	0.01	0.00	-0.00	0.39	81
AOD_{675}	0.01	0.00	0.00	0.24	94
AOD_{870}	0.01	0.00	-0.00	0.23	78
AOD_{1020}	0.03	0.01	0.02	0.18	4
$AE_{400-675}$	1.02	0.81	0.42	0.24	-

2.3.2 ILP with new SVA

Using the data from a solar disk scan performed on 28 September, a new set of SVA values have been computed for the UVEG Prede. The standard ILP algorithm has been then applied to obtain a new set of calibration coefficients based on these new SVA values. As previously mentioned, this recalculation is intended to account for filter degradation over time. With this adjustment, the 340 nm channel can be included again in the analysis.

The results of the intercomparison between the UVEG Prede and the other instruments are shown in Table 7 and in Figures 13a, 13b, 14a and 14b. Overall, the compatibility between the instruments does not show a significant improvement. Although the correlation coefficient increases slightly for some channels (e.g. 675 and 870 nm), the percentage of AOD differences falling within the WMO limits does not necessarily improve (see Figure 14b and Table 7c). For instance, in this analysis 54% of the AOD_{870} differences lie within the limits, whereas in the previous case (Subsection 2.3.1), the traceability of the 870 nm channel is higher, with 78% of the AOD_{870} differences within the WMO interval.

Finally, a new set of calibration coefficients is obtained by applying a new version of the ILP algorithm developed by Gaurav Kumar. In this calculation, the 340 nm channel is excluded to prevent it from affecting the calibration of the remaining channels. The results of the corresponding intercomparison are presented in Table 2. In this case, an overall improvement is observed with respect to the standard ILP calibration (Table 5). When compared with the calibration based on the new SVA values, no substantial improvement is found. Although the correlation values in Table 7 are slightly better, the improvement in AOD traceability achieved with the modified ILP method is particularly remarkable. Additionally, the seasonal dependence of the calibration coefficients and the sensitivity of the ILP method to this seasonality must be considered. Therefore, further improvements in the performance of the new ILP method are expected once the post-campaign calibration is considered. For this reason, the results presented here should be regarded as preliminary.

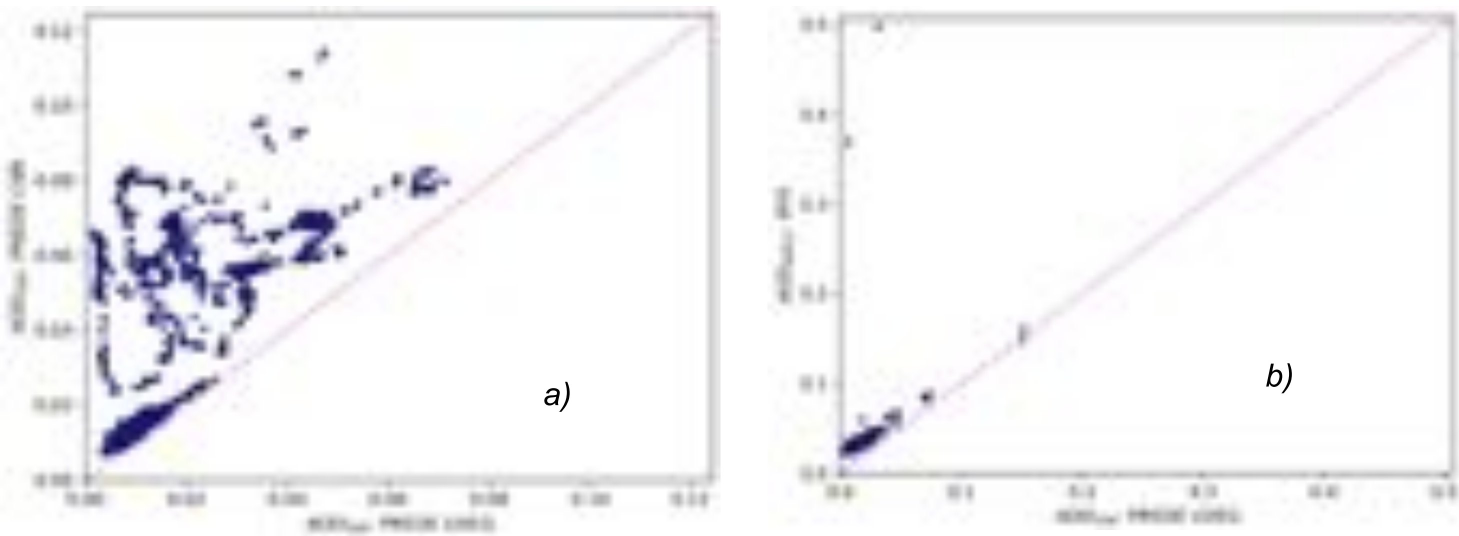

Figure 13: Scatter plot from the comparison of the AOD_{500} retrieved by the UVEG Prede and the (a) CNR Prede; (b) PFR.

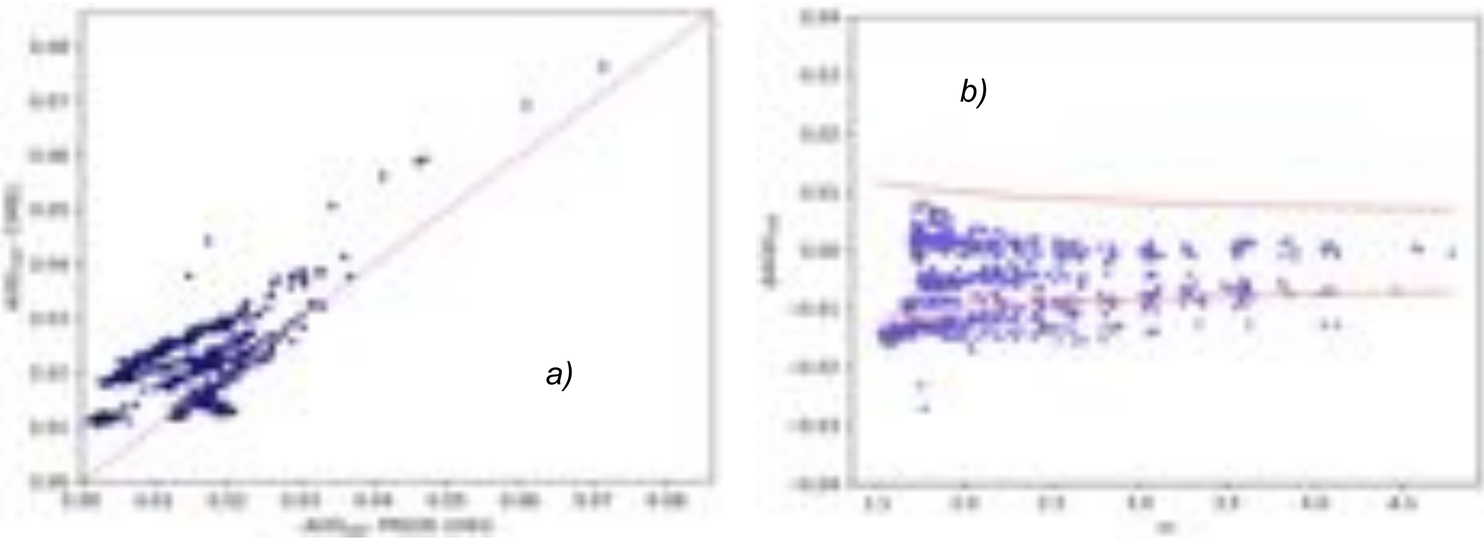

Figure 14: (a) Scatter plot from the comparison of the AOD_{500} retrieved by the UVEG Prede and the Davos Cimel. (b) AOD_{500} differences for the Cimel and the UVEG Prede as a function of the optical air mass. Upper and lower WMO limits are also indicated.

Table 7: Summary of the statistical parameters defined in Eq. 1-5 applied to the comparison of the AOD and AE from the UVEG Prede with the values from the other instruments, at the available wavelengths (see Table 1): (a) UVEG Prede-CNR Prede; (b) UVEG Prede-PFR; and (c) UVEG Prede-Cimel. The standard ILP with a re-calculated SVA based on measurements performed on 28 September has been used in the computation of the UVEG Prede's calibration coefficients.

UVEG Prede-CNR Prede					UVEG Prede-SE SMHI PFR				
a)	$RMSE$	$std(\delta)$	MBD	R^2	b)	$RMSE$	$std(\delta)$	MBD	R^2
AOD_{340}	0.03	0.02	0.02	0.35					
AOD_{400}	0.03	0.02	-0.02	0.35					
AOD_{500}	0.03	0.02	-0.03	0.26	AOD_{500}	0.03	0.02	-0.02	0.19
AOD_{675}	0.04	0.02	-0.03	0.15					
AOD_{870}	0.05	0.02	-0.04	0.05	AOD_{870}	0.03	0.03	-0.01	0.21
AOD_{1020}	0.11	0.03	-0.10	0.29					
$AE_{400-500}$	2.84	1.55	2.38	0.06					
$AE_{400-675}$	1.07	0.46	0.97	0.17	$AE_{400-675}$	1.96	1.14	1.57	0.33
$AE_{400-870}$	1.92	1.01	1.63	0.18					

UVEG Prede-Davos Cimel					
c)	$RMSE$	$std(\delta)$	MBD	R^2	WMO (%)
AOD_{340}	0.05	0.02	0.04	0.06	4
AOD_{500}	0.01	0.01	-0.01	0.39	63
AOD_{675}	0.01	0.00	-0.00	0.26	97
AOD_{870}	0.01	0.00	-0.00	0.30	54
AOD_{1020}	0.03	0.01	0.02	0.20	4
$AE_{400-675}$	1.18	0.83	0.82	0.36	-

3. Summary: future needs

This report summarises the results obtained from the intercomparison of AOD and AE values retrieved from measurements performed by different sun-sky radiometers (Cimel, Prede POM-01 and PFR) during the FRC VI campaign, held in Davos (Switzerland) at the PMOD/WRC from 22 September to 10 October. Overall, a good agreement in AOD has been found between PFR and Cimel products. In contrast, larger discrepancies have been observed for the Prede, mainly associated with the 1020 nm channel (and with the 340 nm channel in the case of the UVEG Prede). These issues are hypothesised to be related to filter degradation, although a more exhaustive analysis is required. This will be carried out once the instruments are returned to their respective sites and the post-campaign calibrations are performed.

On the other hand, the AE comparison did not yield successful results. Since AE is derived from AOD, it will be associated with higher errors. Additionally, due to limitations in the available channels, the AE could not be calculated using a common wavelength range for all instrument. As a result, larger discrepancies in AE are expected.

An additional study was carried out to evaluate the performance of the ILP calibration method. The results clearly show that the determination of the calibration coefficients has a strong impact on the quantities derived from raw measurements. Four calibrations approaches were tested: the standard ILP, the standard ILP excluding the 340 nm channels (due to its poor behaviour), the standard ILP using newly computed SVA values to account for filter degradation, and the ILP version by Gaurav Kumar. The latter two yielded the best results in terms of statistical parameters, correlation coefficients and traceability.

This work has been carried out within the framework of a STSM grant entitled: *Comparison of AOD and aerosol retrievals collected during the FRC-VI campaign in Davos and validation of improved data processing and calibration algorithms,* which enabled the grantee to attend the FRC VI campaign. The results obtained are planned to be included in the applicant's PhD thesis, and aim to be published in a future research article. Furthermore, these results have laid the foundation for further studies and collaborations. The data will be reprocessed, including the additional days of measurements corresponding to the extension of the FRC-VI, taking into account post-calibration, so the results are expected to improve. Furthermore, further research will be necessary to shed light on the behaviour of the 1020 nm channels for both Prede (and the 340 nm channel for UVEG Prede), and further more approaches to improve ILP-based calibration will be proposed and tested.

On the other hand, a potential future collaboration with the aim of homogenise Prede, Cimel and PFR AOD and AE retrievals has been established, and will be a future project in line with the objectives of HARMONIA.

The objectives and results obtained in this project are within the scope of WG1 and WG2, and the dataset will be useful for an uncertainty study to be carried out in order to contribute to Deliverable 2.4 of WG2.

4. References

- Campanelli, M., Nakajima, T., & Olivieri, B. (2004). Determination of the solar calibration constant for a sun-sky radiometer: proposal of an in-situ procedure. Applied optics, 43(3), 651–659. https://doi.org/10.1364/ao.43.000651
- Holben, B. N., Eck, T. F., Slutsker, I., Tanré, D., Buis, J. P., Setzer, A., Vermote, E., Reagan, J. A., Kaufman, Y. J., Nakajima, T., Lavenu, F., Jankowiak, I., & Smirnov, A. (1998). AERONET—A federated instrument network and data archive for aerosol characterization. Remote Sensing of Environment, 66(1), 1–16. https://doi.org/10.1016/S0034-4257(98)00031-5
- Nakajima, T., Campanelli, M., Che, H., Estellés, V., Irie, H., Kim, S.-W., Kim, J., Liu, D., Nishizawa, T., Pandithurai, G., Soni, V. K., Thana, B., Tugjsurn, N.-U., Aoki, K., Go, S., Hashimoto, M., Higurashi, A., Kazadzis, S., Khatri, P., Kouremeti, N., Kudo, R., Marenco, F., Momoi, M., Ningombam, S. S., Ryder, C. L., Uchiyama, A., and Yamazaki, A.: An overview of and issues with sky radiometer technology and SKYNET, Atmos. Meas. Tech., 13, 4195–4218, https://doi.org/10.5194/amt-13-4195-2020
- Sinyuk, A., Holben, B. N., Eck, T. F., Giles, D. M., Slutsker, I., Korkin, S., Schafer, J. S., Smirnov, A., Sorokin, M., and Lyapustin, A.: The AERONET Version 3 aerosol retrieval algorithm, associated uncertainties and comparisons to Version 2, Atmos. Meas. Tech., 13, 3375–3411, https://doi.org/10.5194/amt-13-3375-2020